Simplified Extended Kalman Filter Observer for SOC Estimation of Commercial Power-Oriented LFP Lithium Battery Cells

4 authors, including:

Tarun Huria
Università di Pisa
12 PUBLICATIONS   **296** CITATIONS

SEE PROFILE

Massimo Ceraolo
Università di Pisa
70 PUBLICATIONS   **1,865** CITATIONS

SEE PROFILE

Javier Gazzarri
The MathWorks, Inc
25 PUBLICATIONS   **424** CITATIONS

SEE PROFILE

Simplified Extended Kalman Filter Observer for SOC Estimation of Commercial Power-Oriented LFP Lithium Battery Cells

Tarun Huria and Massimo Ceraolo
Università di Pisa

Javier Gazzarri and Robyn Jackey
MathWorks

ABSTRACT

The lithium iron phosphate (LFP) cell chemistry is finding wide acceptance for energy storage on-board hybrid electric vehicles (HEVs) and electric vehicles (EVs), due to its high intrinsic safety, fast charging, and long cycle life. However, three main challenges need to be addressed for the accurate estimation of their state of charge (SOC) at runtime:

- Long voltage relaxation time to reach its open circuit voltage (OCV) after a current pulse

- Time-, temperature- and SOC-dependent hysteresis

- Very flat OCV-SOC curve for most of the SOC range

In view of these problems, traditional SOC estimation techniques such as coulomb counting with error correction using the SOC-OCV correlation curve are not suitable for this chemistry.

This work addressed these challenges with a novel combination of the extended Kalman filter (EKF) algorithm, a two-RC-block equivalent circuit and the traditional coulomb counting method. The simplified implementation of the EKF algorithm offers a computationally efficient option for runtime SOC evaluation on-board vehicles. The SOC estimation was validated with experimental data of a current profile contaminated with pseudo-random noise and with an offset in the initial condition. The model rapidly converged to within 4% of the true SOC even with imposed errors of 40% to initial SOC, 24% to current measurement and 6% to voltage measurement.

INTRODUCTION

The LFP olivine has emerged as one of the favored cathode materials for lithium ion batteries, especially for use as a rechargeable energy storage device (RESS) on-board HEVs and EVs, thanks to its high intrinsic safety [1], capacity for fast charging, and long cycle life [2]. Recent research and development advancements in this cell technology, especially the commercial launch of high-power LFP cells, have led to these cells matching the performance of the latest super-capacitors over short time periods (up to 30 seconds).

A metric of great importance for a rechargeable lithium battery pack is the accurate runtime evaluation of its SOC, which is defined as the percentage of the completely extractable charge capacity remaining in the battery. It is akin to the fuel gauge of a conventional vehicle. The SOC indicates the amount of electrical energy remaining in the battery pack that is available to do work. An accurate runtime estimate of the SOC is important for the battery application designers and the battery users. However, the charge capacity of a battery depends upon a number of factors, including average current, discharge time, voltage cut-off limit, electrolyte temperature, aging, and battery storage time [3].

Armed with the confidence that the battery SOC would be determined accurately, the designer is able to efficiently use available battery capacity and reduce over-engineering; enabling the use of smaller and lighter batteries. With an accurate indication of the battery SOC, the user ensures that the battery is not over-charged or under-discharged; and suffers less *range anxiety*. Overall, the battery lasts longer and provides better performance. An accurate SOC is also a very important input for the battery management system.

Over the years, many techniques have been proposed for estimation of the battery SOC, and they generally depend upon the battery chemistry and the final application [4-9]. The most reliable test for establishing the SOC of a battery is to charge or discharge it completely, thus physically reaching 100% or 0% SOC. This test is often adopted for an EV or a PHEV that is charged completely every evening, and allows the onboard SOC estimation algorithm to gain valuable feedback to recalibrate itself. For an HEV, which is never charged from the grid, ampere-hour counting remains the most popular technique. This technique (also called the bookkeeping system or coulomb counting) uses discrete integration of measured current over time as a direct indicator of SOC. Since this integration includes errors in current measurement and battery losses, the result needs to be periodically corrected. The OCV vs. SOC correlation curve is often used to provide points for recalibration. Other techniques such as direct measurement of the cell physical properties, including impedance or internal resistance, are not practical for LFP cells during runtime.

The coulomb counting technique with correction (after rest periods) using an OCV-SOC correlation curve is not practical for cells exhibiting hysteresis since the battery cell takes a long time to reach a steady-state OCV after a current pulse. The problem is aggravated for the LFP batteries that also have a very flat OCV-SOC correlation curve. Current SOC-estimation models are unable to take care of all of these complications. A more robust algorithm is needed to estimate the instantaneous total charge available for work inside an LFP cell. The EKF technique, an adaptive estimator, has emerged as one of the practical solutions to enhance the accuracy of SOC determination, but is complicated and needs heavy computing resources on-board the vehicle [6-8].

This paper presents a novel, simplified implementation of the extended Kalman filter technique that overcomes the practical challenges involved in runtime evaluation of the SOC of commercial high-power LFP cells. Its formulation demands a lower level of resources compared to traditional EKF implementations.

CHALLENGES IN RUNTIME ESTIMATION OF SOC OF LFP CELLS
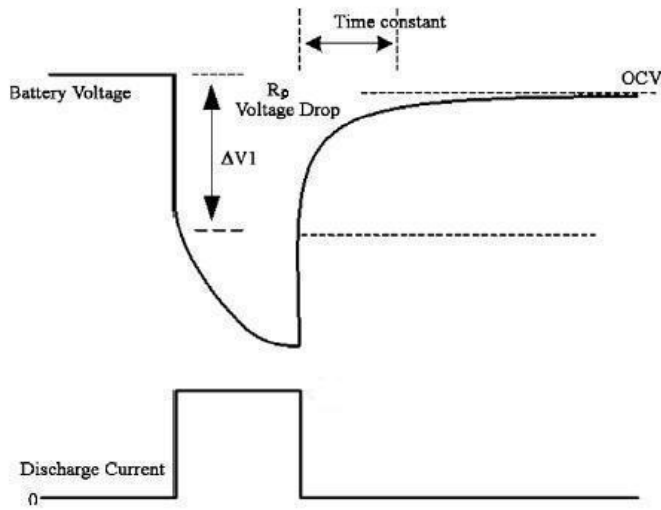
Voltage relaxation time

Figure 1: One pulse of the pulse discharge test (sign convention from Figure 1).

The OCV-SOC correlation curve is often used to correct the current integral errors during runtime. This is usually done when the vehicle has been at rest (with its battery neither charging nor discharging) for a sufficiently long duration (30-60 minutes), and when its battery voltage at the terminals *is assumed to approximate the value of the OCV*. This assumption is valid for most battery chemistries. The authors attempted to validate this assumption for the LFP cells using pulse discharge and charge tests. Under this test, the cell was first completely charged, rested for two hours, and then subjected to ten discharge pulses at 1C rate interspersed by one-hour rest phases until the cell was completely discharged.

Subsequently, the cell was charged using ten charge pulses at 1C rate interspersed by one-hour rest phases until the cell was completely charged. The cell was then allowed to rest for 13 hours. A schematic of one pulse of the discharge test is shown in Figure 1. Figure 2 presents the cell current and terminal voltage measurements during the complete pulse discharge and charge experimental test.
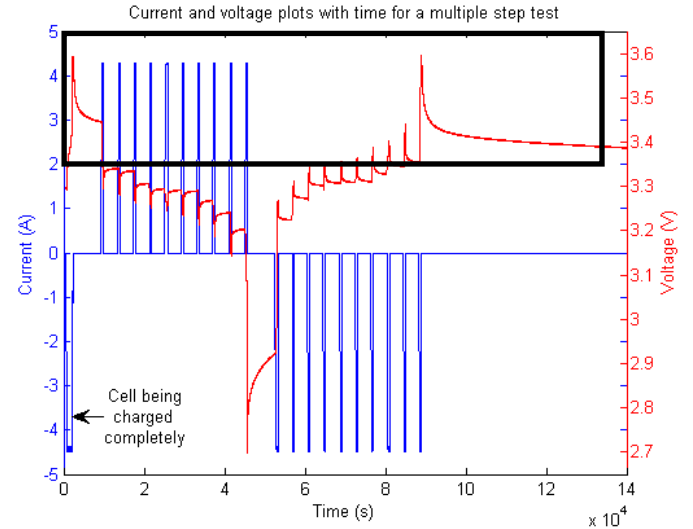

Figure 2: Input current and voltage response for a pulse charge and discharge test (inset in figure 3).
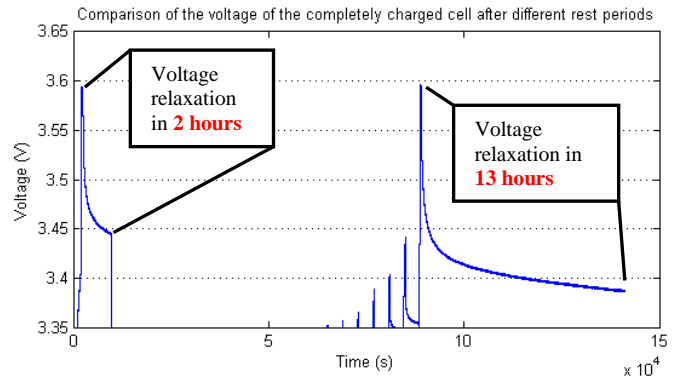

Figure 3: Inset from figure 2 to highlight the long voltage stabilization time.

The authors' primary interest in the experiment was to validate the assumption that the voltage of the LFP cell relaxes to approximately reach its OCV (as shown in Figure 1) after a long rest of one hour. However, it was observed that after the complete pulse discharge and charge test (Figure 2), when the SOC had reached 100%, the voltage did not relax to its OCV even after 13 hours (Figure 3).

Hysteresis

From the pulse discharge and charge experimental test (Figure 2), the voltage at rest was plotted with respect to the SOC for different times of rest, to estimate the amount of hysteresis in the LFP cells. In fact, the hysteresis is correlated with the long voltage relaxation time, with the level of hysteresis decreasing with the rest period, as seen in Figure 4, due to lithium ion diffusion inside the cell.
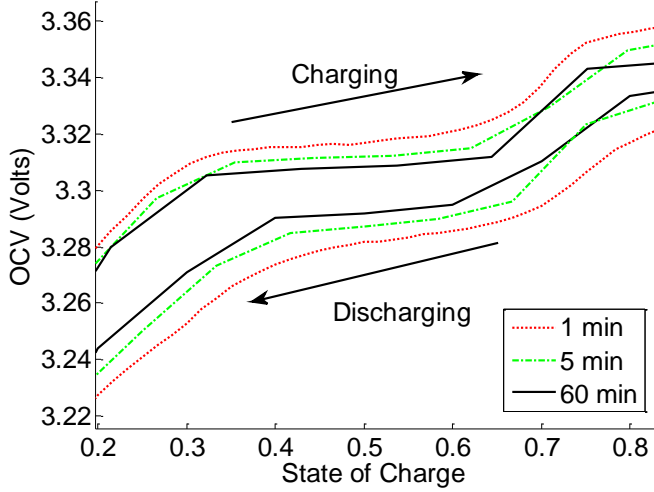

Figure 4: Hysteresis decreases with increasing rest time between pulses (legend in minutes) in the multiple-step test conducted on the LFP cell (20°C). Hysteresis with rest time beyond 60 minutes was excluded from this figure.

This shows that hysteresis depended on time. A second pulse discharge and charge experimental test at a lower temperature of 0°C showed that both the voltage relaxation time was larger and the hysteresis was more pronounced.

Flat OCV-SOC relationship

The pulse discharge and charge tests also produced the OCV-SOC correlation curve for the LFP cell as shown in Figure 5. The curve was nearly flat for SOC levels between 40% and 60%. Moreover, for the entire length of the SOC window from 20% to 80%, the voltage gradient was approximately 0.1V. Even a small error in voltage measurement would have led to a very inaccurate SOC estimate. These observations highlighted the challenge of performing corrections to the coulomb counting technique using the OCV-SOC correlation.
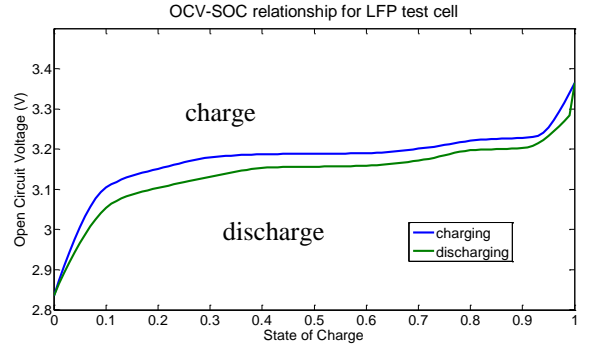

Figure 5: Flat OCV-SOC curve for the LFP cell (20°C) (plotted after a 3-hour rest period).
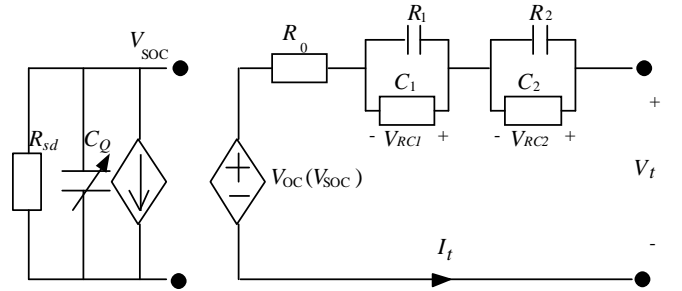
PROPOSED MODEL

Figure 6: Equivalent circuit model of the battery cell (I_t is positive during charge).

To address the challenges posed by the LFP cells as discussed in the section above, the authors proposed the equivalent circuit model shown in Figure 6, based on models already available in the literature [2, 8-12]. In this model, C_Q was the internal capacity of the battery cell ($C_Q=3600C_{nom}$), R_{sd} was a resistance representing the cell self-discharge; V_{SOC} was a voltage ranging between 0 and 1 that models the SOC of the cell, while V_{OC} was the OCV of the cell, a function of the cell SOC. The transient behavior of the cell was captured using three resistors (R_0, R_1 and R_2) and two capacitors (C_1 and C_2). The RC component with the largest time constant accounted for the hysteresis. The system's behavior was described by the following equations:

$$\begin{cases} \dot{V}_{SOC} = \dfrac{-V_{SOC}}{R_{sd}C_Q} + \dfrac{1}{C_Q}I_t \\[2mm] \dot{V}_{RC1} = \dfrac{-V_{RC1}}{R_1 C_1} + \dfrac{1}{C_1}I_t \\[2mm] \dot{V}_{RC2} = \dfrac{-V_{RC2}}{R_2 C_2} + \dfrac{1}{C_2}I_t \\[2mm] V_t = V_{OC} + R_0 I_t + V_{RC1} + V_{RC2} \end{cases} \tag{1}$$

Although the cell SOC was dependent upon the internal cell temperature and the average discharge current rate, this paper presents a simplified approach using an isothermal algorithm because its main purpose is to present the EKF-based methodology. Temperature variation effects will be the subject of a future publication.

Experimental pulse discharge and charge tests were conducted on a 4.4 Ah commercial high-power LFP cell at 20°C to estimate the model parameters using a program built with MATLAB, Simulink, and Simscape. Under this procedure, the LFP cell was first completely charged and then subjected to ten 1C discharge pulses interspersed by one-hour rest phases until the cell was completely discharged. Then the cell was charged using ten 1C charge pulses interspersed by one-hour rest phases until the cell was completely charged.

EXTENDED KALMAN FILTER APPROACH

The Kalman filter is the optimum state estimator for a linear system. For nonlinear systems (in the present case the nonlinearity is given by the OCV-SOC correlation) a linearization process takes place at each time step to approximate the nonlinear system as a linear time varying (LTV) system. This technique is often referred to as extended Kalman filter (EKF) [6-8]. It inherits the ability of the Kalman filter to estimate the best possible values of the inputs containing unmeasured noise. The Appendix describes the basics of EKF in the context of this work.

The EKF was implemented using the equivalent circuit model of Figure 6 with the Simulink model topology shown in Figure 7 to evaluate the SOC at runtime. The voltage and current measured at the battery terminals constituted the input to the SOC evaluation system.

The model was comprised of three main subsystems:

1. Lithium Cell (1R+2RC without Voc): This was the dynamic LTV system simulating the battery transient behavior with parameters that were functions of SOC. These equations were implemented in Simscape with the equivalent circuit of Figure 8. Here, the input port *Ibatt* provided the experimentally measured current. The input port *SOC* provided the corrected estimate of SOC. The output V_{RC} was the calculated potential drop across the branches R_0, R_1-C_1, and R_2-C_2 from the equivalent circuit in Figure 6. The implementation of this subsystem using Simscape is shown in Figure 8.
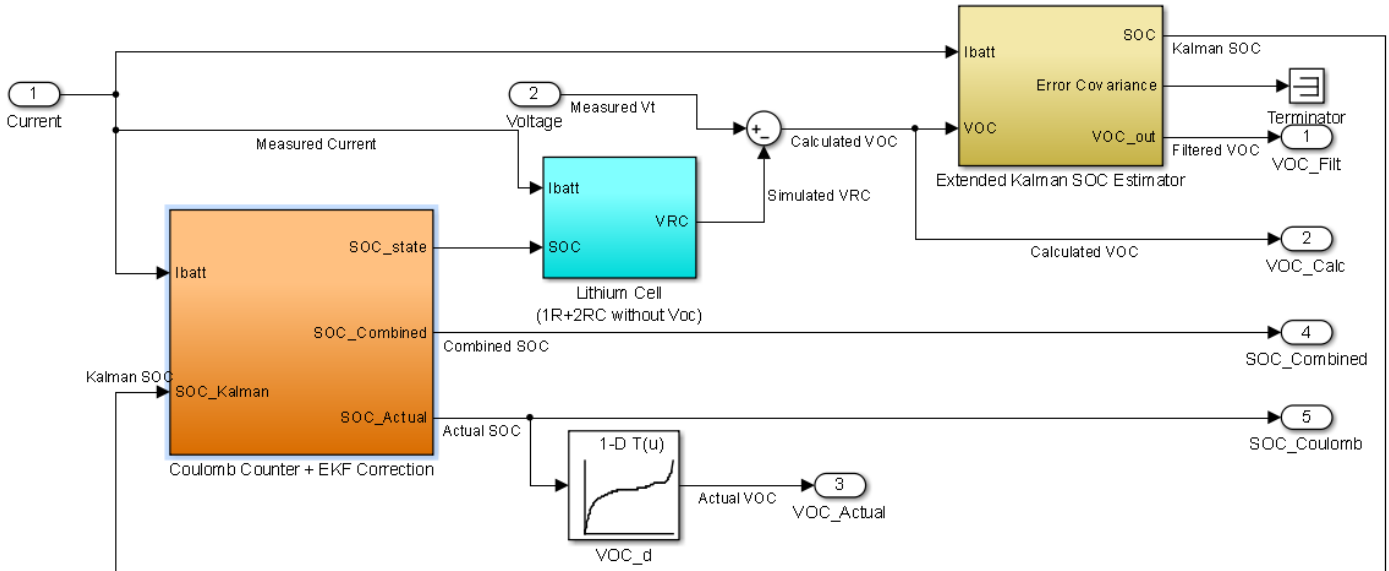

Figure 7: Schematic of the model system architecture in Simulink and Simscape.
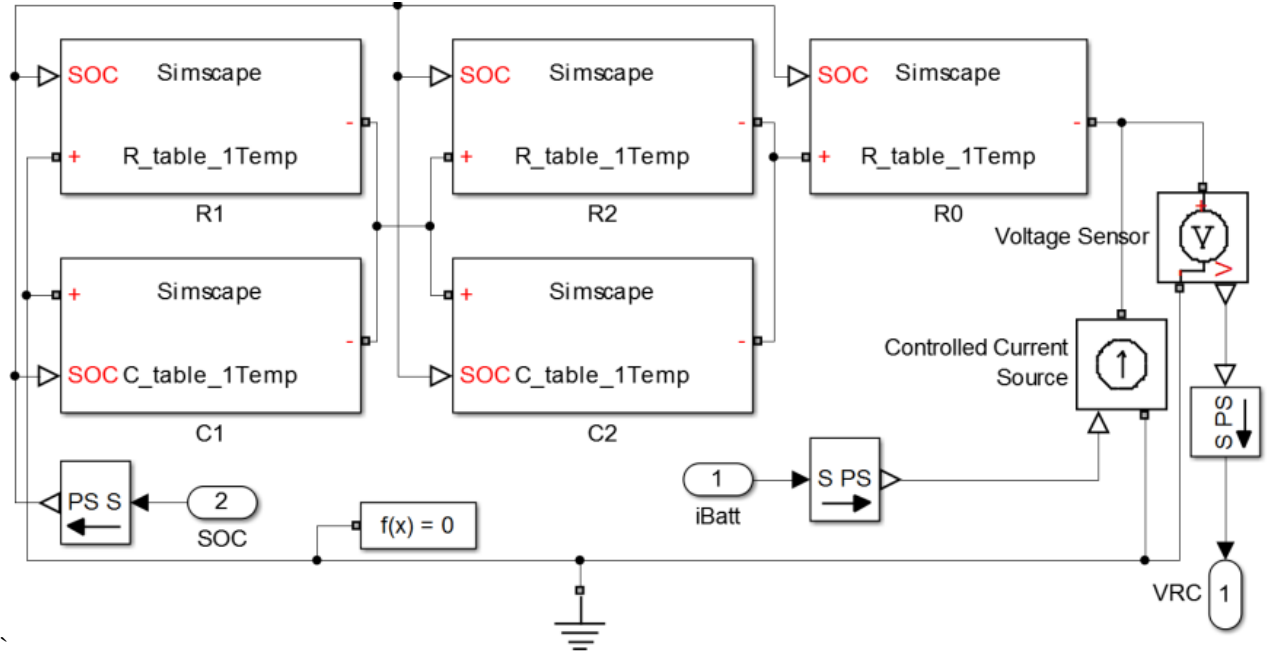
Figure 8: Equivalent circuit model for an LFP cell with two parallel RC branches and a series resistor.

2. Extended Kalman SOC Estimator: This block implemented the EKF. The input port *Ibatt* provided the experimentally measured current. The input port *VOC* provided the estimate of true open-circuit voltage. The true open-circuit voltage *VOC* was calculated as the difference between measured terminal voltage (V_t) and *VRC*, the simulated voltage across the equivalent circuit's R-C network shown in Figure 8. The output port *SOC* was an output of the EKF algorithm. The state equations of the EKF are shown in Equation 2:

$$\begin{cases} x_{k+1} = a_1 x_k + b_1 u_k \\ y_k = f(x_k) \\ x = V_{SOC} \\ u_k = I_t \\ y = V_{OC} \\ a_1 = e^{-t/R_{sd}C_Q} \\ b_1 = R_{sd}\left(1 - e^{-t/R_{sd}C_Q}\right) \end{cases}$$

(2)

where $f(x_k)$ was a non-linear V_{SOC}-V_{OC} correlation function to handle the hysteresis. The actual OCV followed both the major hysteresis loops (0 to 100% SOC during charging and discharging) and the minor loops (small charge-discharge cycles during a larger overall charge or discharge). This non-linear behavior could not be accurately modeled using linear elements such as RC blocks; hence the hysteresis was modeled using equation 3:

$$\frac{dV_{OC}(V_{SOC})}{dV_{SOC}}$$
$$= \begin{cases} \frac{dV_{OC_{ch}}(V_{SOC})}{dV_{SOC}} + k\left(V_{OC_{ch}}(V_{SOC}) - V_{oc}(V_{SOC})\right), & \frac{dV_{SOC}}{dt} > 0 \\ 0 & \frac{dV_{SOC}}{dt} = 0 \\ \frac{dV_{OC_{disch}}(V_{SOC})}{dV_{SOC}} + k\left(V_{OC_{disch}}(V_{SOC}) - V_{oc}(V_{SOC})\right), & \frac{dV_{SOC}}{dt} < 0 \end{cases}$$

(3)

where $V_{OCch}(V_{SOC})$ and $V_{OCdisch}(V_{SOC})$ were the OCV-SOC relationships for charge and discharge respectively on the major loops, and *k,* the hysteresis factor, was the parameter regulating the transition rate between them. The value of *k* was obtained by inspection by minimizing the difference between the experimental and simulated V_{OC} vs. SOC curves. $V_{OC}(V_{SOC})$ is the instantaneous value of the OCV on the minor loop. Other variables are defined in the Abbreviations section.

3. Coulomb Counter + EKF Correction: This block implemented the integration of measured current *Ibatt* to continuously track changes to the battery SOC. The coulomb counter was recalibrated with the EKF SOC estimate only every ten minutes, to reduce the computing requirements. The output *SOC_Actual* was the accurately measured SOC used for validation.

MODEL SIMULATION AND VALIDATION

For validating the model, the battery of a hybrid electric vehicle was simulated running a modified NEDC cycle (Figure 9) in an urban environment (the maximum speed of

the vehicle was limited to 80 km/h instead of 100 km/h in the extra-urban part of the cycle). The battery current and voltage were scaled down to the cell level. This modified NEDC profile was then experimentally applied across the LFP cell.
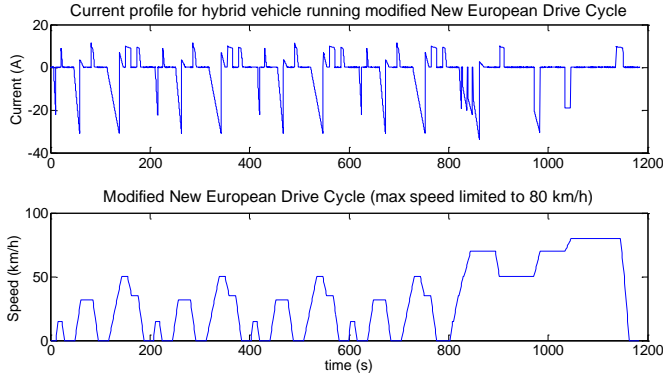

Figure 9: Modified New European Drive Cycle and its simulated current profile (scaled to cell level) in a hybrid vehicle.

The assessment of the EKF algorithm required a comparison of the predicted SOC with the "real" SOC measured accurately in laboratory conditions. This was accomplished via coulomb counting with cell current measured using lab-grade instruments, with the following accuracy:

Maximum voltage error: ±0.035% of full scale
Maximum current error: ±0.06% of full scale

In addition, probing current and voltage directly at the cell terminals further helped keep experimental errors to a minimum.

For the EKF algorithm to be of practical use, it should be implementable with relatively inexpensive measurement hardware. In view of this requirement, the algorithm was contaminated with artificially added offset and proportional errors to both voltage and current measurements, to mimic the output of standard, relatively inexpensive sensors, as follows:

$$I_{\text{EKF}} = 0.4\, Amp + 1.15 I_{\text{lab}}$$
$$V_{\text{EKF}} = 0.04\, Volt + 1.02\, V_{\text{lab}} \tag{4}$$

In addition, the initial SOC for the EKF-based model was set at 20% higher than the actual experimental SOC. Thus, although the initial cell SOC was 50% (cell charged completely, and then discharged at 1C current for 30 minutes), the EKF-based estimator was provided with an initial estimated SOC of 70% to verify model convergence to the actual value within a reasonable period of time.

Figure 10 shows that the SOC estimated by the proposed model converged to the true value of the SOC (measured experimentally) in approximately three hours using a sequence of NEDC cycle repetitions. It is also worth mentioning that

since the EKF-based algorithm always assumed noise in the system, the estimated SOC would approach but never exactly match the true SOC value.
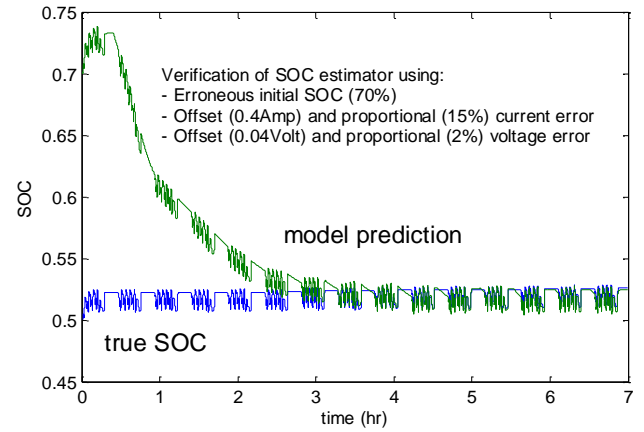

Figure 10: The SOC predicted by the model (green) converged to the true SOC value (blue) in approximately three hours from an artificially erroneous initial condition, and offset and proportional errors in current and voltage.

In a second validation example, the model was simulated with five different input currents with different levels of artificially added error and with the resulting discrepancy between the simulated and true SOC of less than 4%, shown in Figure 11.
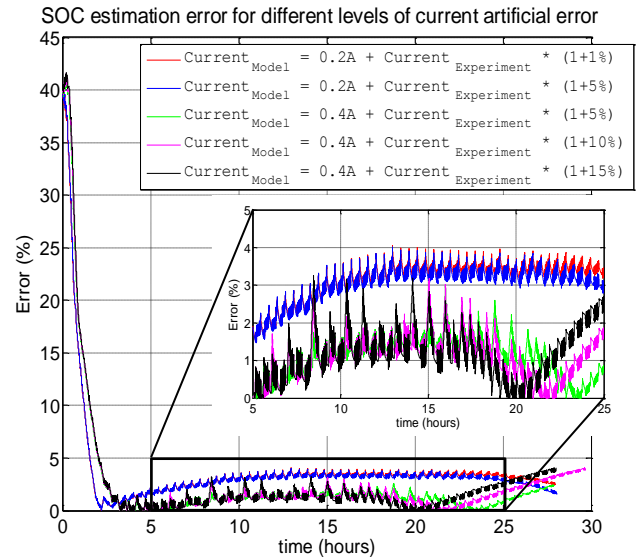

Figure 11: Percentage error in runtime SOC estimation by EKF-based model for different levels of initial error in input current (no voltage error).

Based on this result, the authors concluded that the EKF-based SOC evaluator successfully overcame the challenges posed by the LFP cell chemistry.

SUMMARY/CONCLUSIONS

This work presented a simplified EKF-based algorithm that used a combination of voltage and current measurements with a dynamic model of battery dynamics. A simpler SOC-OCV correlation was unsuitable for LFP cells because of long voltage relaxation time and hysteresis, combined with a very flat SOC-OCV relationship. The EKF-based algorithm proposed in this work predicted SOC within 4% of the value measured using very accurate lab-grade equipment, even in the presence of artificially added errors to mimic commercial-grade sensor measurements.

The coulomb counting was corrected every ten minutes (instead of after every measurement like in state-of-the-art EKF procedures) with the SOC value predicted by the simplified EKF algorithm. This reduced the computing requirements that would be required for real-time SOC evaluation onboard a vehicle.

REFERENCES

1. Scrosati, B. and Garche, J. "Lithium batteries: Status, prospects and future," *J. Power Sources*, 195(9): 2419-2430, 2010, doi:10.1016/j.jpowsour.2009.11.048.
2. Park, Ok Kyung, Yonghyun Cho, Sanghan Lee, Ho-Chun Yoo, Hyun-Kon Song, and Jaephil Cho. "Who will drive electric vehicles, olivine or spinel?" *Energy & Environmental Science*, 4(5):1621-1633, 2011, doi:10.1039/C0EE00559B.
3. Huria, T., Ceraolo, M., Gazzarri, J., Jackey, R., "High fidelity electrical model with thermal dependence for characterization and simulation of high power lithium battery cells," *Electric Vehicle Conference (IEVC), 2012 IEEE International*, March 2012 doi:10.1109/IEVC.2012.6183271.
4. Piller, S., Perrin, M., and Jossen, A., "Methods for state-of-charge determination and their applications", *J. Power Sources*, 96:113-120, 2001, doi:10.1016/S0378-7753(01)00560-2
5. Pop, V., Bergveld, H., Notten, P., and Regtien, P. "State-of-the-art of battery state-of-charge determination", *Meas. Sci. Technol.*, 16 R93-R110, 2005, doi:10.1088/0957-0233/16/12/R01
6. G. L. Plett, "Extended Kalman filtering for battery management systems of LiPB-based HEV battery packs: Part 1. Background," *J. Power Sources*, 134(2): 252-261, 2004, doi:10.1016/j.jpowsour.2004.02.031.
7. G. L. Plett, "Extended Kalman filtering for battery management systems of LiPB-based HEV battery packs: Part 2. Modeling and identification," *J. Power Sources*, 134(2): 262-276, 2004, doi:10.1016/j.jpowsour.2004.02.032.
8. G. L. Plett, "Extended Kalman filtering for battery management systems of LiPB-based HEV battery packs: Part 3. State and parameter estimation," *J. Power Sources*, 134(2): 277-292, 2004, doi:10.1016/j.jpowsour.2004.02.033.
9. Chen, M. and Rincon-Mora, G.A. , "Accurate electrical battery model capable of predicting runtime and I-V performance," *IEEE Transactions on Energy Conversion*, vol.21, no.2, pp. 504- 511, June 2006 doi:10.1109/TEC.2006.874229.
10. Ceraolo, M., "New Dynamical Models of Lead-Acid Batteries", *IEEE Transactions on Power Systems*, 15(4):1184-1190, 2000, doi:10.1109/59.898088.
11. Ceraolo, M., Barsali, S., "Dynamical models of lead-acid batteries: Implementation issues," *IEEE Transactions on Energy Conversion*, 17(1):16-23, 2002, doi:10.1109/60.986432.
12. Huria, T., "Rechargeable lithium battery energy storage systems for vehicular applications", http://etd.adm.unipi.it/t/etd-04262012-182954/, Ph.D. thesis, Department of Energy and Systems Engineering, University of Pisa, 2012.

ACKNOWLEDGMENTS

ABBREVIATIONS

1C	A constant current rate of discharge or charge in amperes equal to the battery's nominal capacity in ampere-hours.
C_n	Capacitor n
C_Q	Capacitor emulating the cell charge capacity
EKF	Extended Kalman filter
I_t	Current measured at cell terminals (A)
k	Hysteresis factor (k=0.1384, obtained by minimizing the difference between the experimental and simulated V_{OC} vs. SOC)
LFP	Lithium iron phosphate
LTV	Linear time varying system
OCV	Open circuit voltage (V)
R_n	Resistor n
R_{sd}	Resistor emulating the cell self-discharge
RESS	Rechargeable energy storage system
SOC	State of charge (0 to 1)
V_{OC}	Open circuit voltage (V)
$V_{OC_{ch}}$	Open circuit voltage during charging (V)
$V_{OC_{disch}}$	Open circuit voltage during discharging (V)
V_{SOC}	Voltage equal to the SOC of the cell (0 to 1V)
V_t	Voltage measured at cell terminals (V)

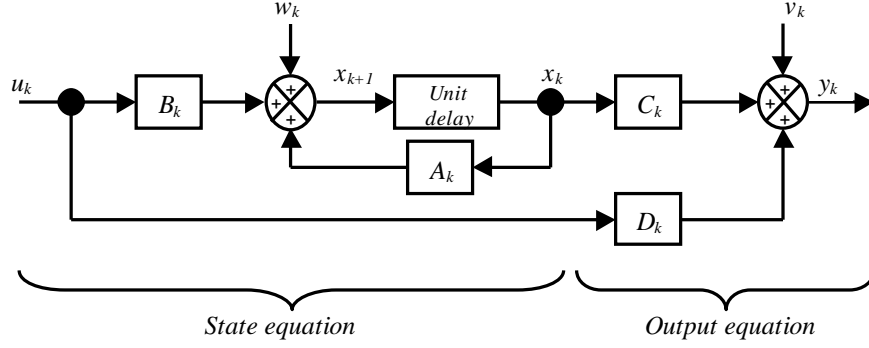# APPENDIX: KALMAN FILTER AND EXTENDED KALMAN FILTER

Figure 1: Block diagram of the Kalman filter in state-space form.

The general framework of the Kalman filter consists of two equations:

$$x_{k+1} = A_k x_k + B_k u_k + w_k$$

(1)

$$y_k = C_k x_k + D_k u_k + v_k$$

(2)

Here, x_k is the system state vector at time index k, and equation 1 is called the *state equation* or *process equation* as it captures the system dynamics. The input to the system is u_k which is known or can be measured. However, the measurement could result in errors, assumed to be stochastic process noise, w_k, which cannot be measured and affects the state of the system.

Equation 2 models the output of the system y_k, in terms of the input, the state vector and the noise in the measurement of the output, v_k. This equation is also called the *measurement equation* or the *output equation*.

Both w_k and v_k are assumed to be mutually uncorrelated white Gaussian random processes with zero mean and covariance matrices of known values. The equations are initialized by setting the following at k=0

$$\hat{x}_0^+ = E[x_0] \text{ and } \quad \Sigma_{\tilde{x},0}^+ = E[(x_0 - \hat{x}_0^+)(x_0 - \hat{x}_0^+)^T]$$

(3)

where, the superscript T refers to the transpose of the matrix. For k=1,2,3… the following computations are made:

State estimate time update: $\hat{x}_k^- = A_{k-1}\hat{x}_{k-1}^+ + B_{k-1}u_{k-1}$ (4)

Error covariance time update: $\Sigma_{\tilde{x},k}^- = A_{k-1}\Sigma_{\tilde{x},k-1}^+ A_{k-1}^T + \Sigma_w$ (5)

Kalman gain matrix: $L_k = \Sigma_{\tilde{x},k}^- C_k^T [C_k \Sigma_{\tilde{x},k}^- C_k^T + \Sigma_v]^{-1}$ (6)

State estimate measurement update: $\hat{x}_k^+ = \hat{x}_k^- + L_k[y_k - C_k\hat{x}_k^- - D_k u_k]$ (7)

Error covariance measurement update: $\Sigma_{\tilde{x},k}^+ = (I - L_k C_k)\, \Sigma_{\tilde{x},k}^-$ (8)

The linear discrete-time Kalman filter computes two estimates – an *a priori* estimate, $\hat{x}_k^-$, based on the prior state estimate computed in the previous iteration, $\hat{x}_{k-1}^+$. This estimate is computed *before* any system measurements are made and is denoted with a superscript "–". After the system measurements of the input u_k and output y_k, the second estimate $\hat{x}_k^+$ is more accurate and is denoted with a superscript "+". Thus, at every measurement interval, the Kalman filter first *predicts* the value of the present state, system output and error covariance: and then *corrects* the state estimate and error covariance. The prediction step is called the *time update* while the

correction step is also known as the *measurement update*. The error difference between the predicted output and the actual output represents the new information and is called the *innovation process*.

The Kalman filter then optimizes the minimum squared error estimate $\hat{x}_k$ of the true state x_k for the entire set of observed data $\{u_0, u_1...u_k\}$ and $\{y_0, y_1...y_k\}$ by solving:

$$\hat{x}_k = \arg\min \mathrm{E}[(x_k - \hat{x})^T(x_k - \hat{x})] \text{ for all inputs} \tag{9}$$

Since the Kalman filter can only be used on linear systems, for nonlinear systems, the extended Kalman filter (EKF) is used by using a linearization process. The nonlinear system is depicted as:

$$x_{k+1} = f(x_k, u_k) + w_k \tag{10}$$

$$y_k = g(x_k, u_k) + v_k \tag{11}$$

where, w_k and v_k are white Gaussian stochastic processes with zero mean and covariance matrices Σ_w and Σ_v respectively. The functions $f(x_k, u_k)$ and $g(x_k, u_k)$ are linearized using a Taylor-series expansion, assuming that they are differentiable at all operating points.

Here, the elements of the state vector matrix are defined as:

$$\hat{A}_k = \left.\frac{\partial f(x_k, u_k)}{\partial x_k}\right|_{x_k = \hat{x}_k^+}, \qquad \hat{C}_k = \left.\frac{\partial g(x_k, u_k)}{\partial x_k}\right|_{x_k = \hat{x}_k^-} \tag{12}$$

The nonlinear state space model can be expressed as:

$$x_{k+1} \approx \hat{A}_k x_k + f(\hat{x}_k, u_k) - \hat{A}_k \hat{x}_k + w_k \tag{13}$$

$$y_k \approx \hat{C}_k x_k + g(\hat{x}_k, u_k) - \hat{C}_k \hat{x}_k + v_k \tag{14}$$

The terms $f(\hat{x}_k, u_k) - \hat{A}_k \hat{x}_k$ and $g(\hat{x}_k, u_k) - \hat{C}_k \hat{x}_k$ replace the terms $B_k u_k$ and $D_k u_k$ in the standard Kalman filter. The initialisation of the equations at k=0 are made as follows:

$$\hat{x}_0^+ = \mathrm{E}[x_0] \quad \text{and} \quad \Sigma_{\tilde{x},0}^+ = \mathrm{E}[(x_0 - \hat{x}_0^+)(x_0 - \hat{x}_0^+)^T] \tag{15}$$

where, again the superscript T indicates the transpose of the matrix. For k=1,2,3... the following computations are made as follows:

State estimate time update: $\qquad \hat{x}_k^- = f(\hat{x}_{k-1}^+, u_{k-1})$ (16)

Error covariance time update: $\quad \Sigma_{\tilde{x},k}^- = \hat{A}_{k-1} \Sigma_{\tilde{x},k-1}^+ \hat{A}_{k-1}^T + \Sigma_w$ (17)

Kalman gain matrix: $\qquad\qquad L_k = \Sigma_{\tilde{x},k}^- \hat{C}_k^T [\hat{C}_k \Sigma_{\tilde{x},k}^- \hat{C}_k^T + \Sigma_v]^{-1}$ (18)

State estimate measurement update: $\quad \hat{x}_k^+ = \hat{x}_k^- + L_k[y_k - g(\hat{x}_k^-, u_k)]$ (19)

Error covariance measurement update: $\Sigma_{\tilde{x},k}^+ = (I - L_k \hat{C}_k) \Sigma_{\tilde{x},k}^-$ (20)

The above set of equations can be used to estimate the inner state vector, such as the SOC. The drawbacks of this technique are that it is computationally intensive and needs a good initial estimate.